J Arid Land (2024) 16(3): 355–372
https://doi.org/10.1007/s40333-024-0095-y

Science Press Springer-Verlag

Linkage between precipitation isotopes and water vapor sources in the monsoon margin: Evidence from arid areas of Northwest China

CHEN Fenli[1,2], ZHANG Qiuyan[1,2], WANG Shengjie[1,2*], CHEN Jufan[1,2], GAO Minyan[1,2], Mohd Aadil BHAT[3]

[1] College of Geography and Environmental Science, Northwest Normal University, Lanzhou 730000, China;
[2] Key Laboratory of Resource Environment and Sustainable Development of Oasis of Gansu Province, Northwest Normal University, Lanzhou 730000, China;
[3] School of Ocean and Earth Science, Tongji University, Shanghai 200092, China

Abstract: The isotope composition in precipitation has been widely considered as a tracer of monsoon activity. Compared with the coastal region, the monsoon margin usually has limited precipitation with large fluctuation and is usually sensitive to climate change. The water resource management in the monsoon margin should be better planned by understanding the composition of precipitation isotope and its influencing factors. In this study, the precipitation samples were collected at five sampling sites (Baiyin City, Kongtong District, Maqu County, Wudu District, and Yinchuan City) of the monsoon margin in the northwest of China in 2022 to analyze the characteristics of stable hydrogen (δD) and oxygen ($\delta^{18}O$) isotopes. We analyzed the impact of meteorological factors (temperature, precipitation, and relative humidity) on the composition of precipitation isotope at daily level by regression analysis, utilized the Hybrid Single-Particle Lagrangian Integrated Trajectory (HYSPLIT)-based backward trajectory model to simulate the air mass trajectory of precipitation events, and adopted the potential source contribution function (PSCF) and concentration weighted trajectory (CWT) to analyze the water vapor sources. The results showed that compared with the global meteoric water line (GMWL), the slope of the local meteoric water line (LMWL; $\delta D=7.34\delta^{18}O-1.16$) was lower, indicating the existence of strong regional evaporation in the study area. Temperature significantly contributed to $\delta^{18}O$ value, while relative humidity had a significant negative effect on $\delta^{18}O$ value. Through the backward trajectory analysis, we found eight primary locations that were responsible for the water vapor sources of precipitation in the study area, of which moisture from the Indian Ocean to South China Sea (ITSC) and the western continental (CW) had the greatest influence on precipitation in the study area. The hydrogen and oxygen isotopes in precipitation are significantly influenced by the sources and transportation paths of air mass. In addition, the results of PSCF and CWT analysis showed that the water vapor source areas were primarily distributed in the south and northwest direction of the study area.

Keywords: water vapor; monsoon margin; stable water isotope; transport trajectory; air mass; *d*-excess; $\delta^{18}O$; δD

Citation: CHEN Fenli, ZHANG Qiuyan, WANG Shengjie, CHEN Jufan, GAO Minyan, Mohd Aadil BHAT. 2024. Linkage between precipitation isotopes and water vapor sources in the monsoon margin: Evidence from arid areas of Northwest China. Journal of Arid Land, 16(3): 355–372. https://doi.org/10.1007/s40333-024-0095-y

*Corresponding author: WANG Shengjie (E-mail: wangshengjie@nwnu.edu.cn)
Received 2023-09-20; revised 2024-01-31; accepted 2024-02-07

1 Introduction

As the main input of terrestrial water resources, precipitation is an important part in the hydrological cycle and it is of great significance to economic development and ecological stability in inland areas, especially in arid areas. Although heavy isotopes of hydrogen (δ^2H, also known as δD) and oxygen ($\delta^{18}O$) in precipitation exist with very small absolute amounts, they are very sensitive to environmental changes. They can record the information of water transportation, condensation, exchange, and other atmospheric process while the air mass is transported from its source to the site of precipitation (Craig, 1961; Dansgaard, 1964). As a natural tracer in precipitation, the stable δ^2H and $\delta^{18}O$ isotopes are widely used to study moisture sources (Tan, 2014; Wang et al., 2017; Fang et al., 2022; Geppert et al., 2022; Sun et al., 2023; Tharammal et al., 2023).

Gimeno et al. (2012) summarized the methods available to identify the moisture sources, including the analytical box method, physical tracer (isotope) method, and numerical tracer method. Among them, the physical water vapor tracer method, which includes the vertical and horizontal atmospheric processes, enables the combination of global climate models and Lagrangian models. In recent years, this method has been widely used to analyze the source of water vapor by mapping the movement of air mass containing water vapor (Breitenbach et al., 2010; Chen et al., 2020; Cloux et al., 2021).

In precipitation, stable δ^2H and $\delta^{18}O$ isotopes are components of water molecules, and their composition variations depend on moisture source, meteorological factor, and transportation mode (Gou et al., 2022). The regimes controlling isotope fractionations in precipitation have been concerned by a large number of researchers (Baker et al., 2015; Steen-Larsen et al., 2015; Tang et al., 2017; Espinoza et al., 2021). Due to the large precipitation amount, many studies on the influencing mechanism of water vapor source on precipitation isotope have been conducted in monsoon area. According to the convective activity, cloud formation, and air trajectory in the monsoon area, the researchers examined the influence of various water vapor sources on the variation of isotopes in precipitation on different scales (Cai et al., 2018; Lone et al., 2020). For example, the decrease in the $\delta^{18}O$ value of precipitation on the Tibetan Plateau, China at the beginning of monsoon season (from late May to early June) can be attributed to the changes in water sources (Yao et al., 2013). Moreover, convective processes may change the composition of water vapor isotopes in the source region, and the transport of water vapor also affects the composition of isotopes in precipitation (Lee et al., 2007; Worden et al., 2007; Risi et al., 2008; Kurita, 2013; Moore et al., 2014). From a spatial perspective, the temperature effect, amount effect, and altitude effect are important factors affecting isotope composition (Salamalikis et al., 2016; Jiao et al., 2019; Yang et al., 2019; Pant et al., 2021). However, many studies found an association between the composition of isotopes in precipitation and the location and/or intensity of convection activities in the upper reaches (Zhou et al., 2019). In addition, the falling raindrops undergo isotope fractionation when passing through the unsaturated air, namely secondary evaporation under the cloud base, which changes the composition of isotopes (Chen et al., 2020). The value of deuterium excess (*d*-excess, which is equal to $\delta D - 8\delta^{18}O$) is related to the evaporation rate of precipitation source area, and a high value of *d*-excess usually indicates low relative humidity and intense evaporation (Natali et al., 2022).

Compared with the coastal region dominated by monsoon, the monsoon margin usually has limited precipitation amount with large fluctuation and is usually sensitive to climate change. The concept of "monsoon triangle" was first proposed by Li et al. (1988) who pointed out that a sensitive triangle area to climate exist in China during the Quaternary period, and the great changes in circulation pattern, vegetation, soil, and climate have been found in the "monsoon triangle" between glacial and interglacial periods. The western vertex of "monsoon triangle" reaches deep into continent, while the other two vertexes are close to sea. Actually, the western vertex corresponds to the monsoon margin. After a long-range transport, air mass sources reaching the monsoon margin are usually complex, and frequent precipitation extremes can be

reported in such an arid climate. In addition, the climate research in the monsoon margin is also an important topic, and the findings from modern precipitation isotopes are necessary basis for paleoclimate proxy. A systemic and synchronous observation network of precipitation isotopes in the monsoon margin not only enhances the understanding of evaporation and condensation in arid condition, but also has great significance for ecological protection and high-quality development in water scarcity areas.

The objectives in this study are to: (1) use the Lagrange method to examine the linkage between the water vapor sources and precipitation stable isotopes ($\delta^{18}O$ and δD) in the monsoon margin in an arid condition; and (2) quantify the influence of different water vapor sources on isotopic characteristics.

2 Data and methodology

2.1 Study area

Here five meteorological stations (Fig. 1) were selected from the margin area of East Asian monsoon (also known as the margin area of "monsoon triangle" or monsoon margin) as sampling sites in this study, including Baiyin City, Kongtong District, Maqu County, and Wudu District in Gansu Province, as well as Yinchuan City in Ningxia Hui Autonomous Region, China. The highest elevation is in Maqu County (3471 m a.s.l.), and the lowest is 1010 m a.s.l. in Yinchuan City (Table 1). The study area has a dry continental monsoon climate, with uneven distribution of annual precipitation and intense evaporation (Kong et al., 2023). The average annual temperature in the study area is 9.29°C, and the average annual precipitation is 394.66 mm, with more rains in summer and autumn, and less rain and snow in spring and winter. This network corresponds to the western vertex of "monsoon triangle" of China (Li et al., 1988).

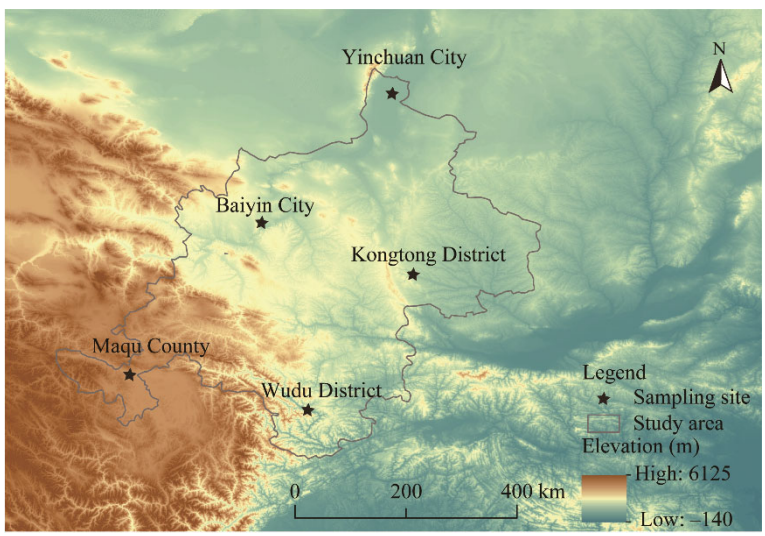

Fig. 1 Location of sampling sites at the margin area of the East Asian monsoon

Table 1 Climate characteristics of the five sampling sites from 1991 to 2020

Sampling site	Latitude	Longitude	Altitude (m)	Temperature (°C)	Precipitation (mm)	Relative humidity (%)
Baiyin City	36°55′N	104°18′E	1719	9.03	210.40	56.00
Kongtong District	35°55′N	106°67′E	1364	9.70	486.40	51.00
Maqu County	34°00′N	102°08′E	3471	2.30	612.30	63.00
Wudu District	33°00′N	104°92′E	1116	15.30	470.40	61.00
Yinchuan City	38°48′N	106°22′E	1010	10.10	193.80	52.00

Note: The latitude and longitude data are the geographical coordinates of the meteorological stations that were used as the sampling sites by this study.

2.2 Isotope data

A funneled polyethylene bottle with a capacity of 1 L was placed at the sampling sites as a precipitation collecting device. To avoid evaporation, we collected the precipitation samples after each precipitation event. In this study, precipitation event was defined as more than 1 mL of water was collected in the bottle. After collection, the collected water samples were transferred to sealed 50 mL polyethylene bottles, and then kept in a cool place. For solid precipitation, it was placed into a zip-locked bag at room temperature after collection, and then transferred to a polyethylene bottle after melting. The basic information of meteorological elements (including temperature, humidity, wind direction, wind speed, etc.) was recorded when precipitation event occurred. A total of 236 precipitation samples were collected at the five sampling sites in the whole year of 2022. The water samples were measured in the Stable Isotope Laboratory, College of Geography and Environmental Science, Northwest Normal University, China The DLT-100 liquid water isotope analyzer (Los Gatos Research, San Jose, the USA) was used to measure the values of ^{1}H, ^{2}H, ^{3}H, ^{16}O, $\delta^{17}O$, and^{18}O. The analysis error of δD value was within ±0.6‰ and that of the $\delta^{18}O$ value was within ±0.2‰ in this study. The values of δD and $\delta^{18}O$ were expressed as one-thousandth of the difference relative to the Vienna Standard Mean Ocean Water (VSMOW) (Zhang et al., 2023):

$$\delta = \frac{R_{\text{sample}}}{R_{\text{standard}}} - 1, \tag{1}$$

where δ is one-thousandth of the difference relative to VSMOW; R_{sample} is the ratio of heavy to light isotopes in water samples, i.e., D/H and $^{18}O/^{16}O$ for δD and $\delta^{18}O$, respectively; and R_{standard} is the corresponding isotopic ratio in VSMOW.

Surface meteorological data including temperature, wind direction, wind speed, and precipitation were obtained from the China Meteorological Data Network (http://data.cma.cn/dat). The upper air meteorological data obtained from the National Centers for Environmental Prediction (http://ready.arl.noaa.gov/archives.php) were used for air mass backward trajectory analysis as well as potential source area analysis.

2.3 Methodology

In this study, Hybrid Single-Particle Lagrangian Integrated Trajectory (HYSPLIT) model was used to simulate the air mass trajectory of precipitation events. The potential source contribution function (PSCF) and concentration weighted trajectory (CWT) were used to analyze the water vapor sources of precipitation air mass.

2.3.1 HYSPLIT model

The HYSPLIT model developed by the National Oceanic and Atmospheric Administration (NOAA) and the Australian Bureau of Meteorology was used to simulate patterns of airflow movement, deposition, and dispersion. It has been widely used to track sources and paths of precipitation air mass. In the model, the Lagrangian method is used for advection and diffusion, and Euler's method is used for concentration calculations (Stohl et al., 2005). MeteoInfo backward trajectory clustering analysis based on the HYSPLIT model was used in the water vapor source analysis (Wang, 2014). The Global Data Assimilation System (GDAS) data were imported into MeteoInfo software (Chinese Academy of Meteorological Sciences, Beijing, China). We conducted backward trajectory simulation for precipitation events in the study area, and then clustered the trajectories obtained.

2.3.2 PSCF

The PSCF analysis is a method used to identify possible source locations based on clustering results of backward trajectory simulation. Considering the environmental significance of *d*-excess (Natali et al., 2022; Chen et al., 2023; Kong et al., 2023; Pérez-Alarcón et al., 2023; Tao et al., 2023), we applied the average *d*-excess value as a threshold to analyze the precipitation potential source area in this study. That is, the trajectories with *d*-excess values higher than the average *d*-excess value were counted as potential trajectories; otherwise, they were not counted as

potential trajectories (Shi et al., 2010; Xie et al., 2022). The PSCF value is the ratio of number of trajectories that pass through a target grid (m) to the number of all trajectories (n), with the following equation:

$$\mathrm{PSCF} = \frac{m}{n}. \tag{2}$$

If the number of trajectories passing through the target grid (m) is too small, the probability function results will deviate from the actual results. To ensure the accuracy of PSCF value, we introduced a weighting factor w defined in Zeng and Hopke (1989) as follows.

$$w_{\mathrm{PSCF}} = \frac{\mathrm{PSCF}}{w}, \tag{3}$$

where w_{PSCF} is the weight of PSCF value.

2.3.3 CWT

Besides PSCF analysis, we also adopted CWT analysis to identify the potential source location of trajectory in this study (Hsu et al., 2003). The spatial distributions of trajectory and corresponding isotopic characteristics were considered in this method (Zannoni et al., 2019; Zhang et al., 2023). The formula for calculating CWT is as follows:

$$C_{ij} = \frac{\sum_{i=1}^{n} C_k \tau_{ijk}}{\sum_{i=1}^{n} \tau_{ijk}}, \tag{4}$$

where C_{ij} is the weighted average of d-excess value in the grid (i, j) (‰/m^3); k is the trajectory; n is the total number of trajectories; C_k is the d-excess value when the trajectory k travels in the grid (i, j); and τ_{ijk} is the duration that the trajectory k stays in the grid (i, j). High CWT value (i.e., C_{ij}) indicates a large potential contribution of a specific location. If the numbers of trajectory endpoint passing through the grid are too small, it will lead to biased results. To ensure the accuracy of CWT value, we used the same weighting factor w as PSCF (Zeng and Hopke, 1989), and the formula is as follows:

$$w_{\mathrm{CWT}} = w \times \mathrm{CWT}. \tag{5}$$

where w_{CWT} is the weight of CWT value.

3 Results

3.1 Isotope characteristics

3.1.1 Spatial and temporal variations of hydrogen and oxygen isotopes

The summer monsoon transports water vapor from the tropical or subtropical oceans to inland areas (Ma et al., 2022). The monsoon moisture usually starts in mid-May, gradually advances northward, and ends completely in mid-October (Bian et al., 2017). During June–September 2022, the lowest monthly precipitation was 2.60 mm (September in Baiyin City) and the highest was 246.90 mm (August in Kongtong District). July and August were periods with relatively frequent precipitation events, and monsoon circulation brought a lot of water vapor to the monsoon margin. The temperature fluctuated between 3.50°C and 29.50°C during June–September 2022, and the average was 18.20°C. Among the sampling sites, the temperature in Maqu County was relatively low, with a fluctuation range of 3.50°C–17.10°C and an average of 11.70°C. This may be mainly because Maqu County has a high altitude with a plateau climate, whose characteristic is long cold winters and short cool summers. The δD value in June–September 2022 ranged from –145.35‰ to 47.18‰, with an average value of –37.79‰, and the δ^{18}O value ranged from –19.34‰ to 7.42‰, with an average value of –5.31‰ (Table 2). These results are within the range of the statistical results of stable hydrogen and oxygen isotopes (–263.20‰–59.00‰ for δD, and –33.40‰–8.50‰ for δ^{18}O) of precipitation in the arid region of Northwest China (Zeng et al., 2020).

Table 2 Statistic values of stable hydrogen (δD), oxygen ($\delta^{18}O$), and deuterium excess (*d*-excess) for each sampling site during June–September 2022

Sampling site	δD (‰)				$\delta^{18}O$ (‰)				*d*-excess (‰)			
	Max	Min	Mean	SD	Max	Min	Mean	SD	Max	Min	Mean	SD
Baiyin City	34.53	–120.02	–17.65	32.84	4.69	–16.02	–2.22	4.49	16.01	–14.37	0.11	8.25
Kongtong District	28.81	–118.99	–40.87	31.95	3.12	–16.37	–6.40	4.18	21.17	–8.88	6.22	6.92
Maqu County	–3.90	–120.68	–71.06	17.36	–2.21	–15.02	–9.38	3.14	18.45	–27.28	3.94	13.85
Wudu District	47.18	–84.22	–28.13	29.81	7.42	–11.37	–3.79	4.05	20.67	–25.25	2.16	9.81
Yinchuan City	35.22	–145.35	–31.25	38.75	5.96	–19.34	–4.76	5.23	22.07	–20.11	7.21	9.97
Total	47.18	–145.35	–37.79	34.94	7.42	–19.34	–5.31	4.79	19.67	–19.18	3.93	11.27

Note: Max, maximum value; min, minimum value; SD, standard deviation.

3.1.2 Local meteoric water line (LMWL)

Craig (1961) found a linear correlation between δD and $\delta^{18}O$ isotopes in natural water samples with the equation of $\delta D=8.00\delta^{18}O+10.00$, also known as the global meteoric water line (GMWL). Rozanski et al. (1993) updated the line using the global precipitation isotope data as $\delta D=8.17\delta^{18}O+10.56$. According to the 1815 months of observed precipitation isotope data in China, the Chinese meteoric water line is $\delta D=7.80\delta^{18}O+8.70$ (Wang et al., 2022), and the nationwide grid isotope data with finer spatial resolution (the number of grids is 431,136) show an equation as $\delta D=7.40\delta^{18}O+5.50$ (Wang et al., 2022), both the lines are generally similar to the global mean.

Due to the differences in climatic conditions, the isotopic composition of precipitation spatially varies. Strong evaporation causes the water line equation to deviate from the slope of 8 of GMWL. The higher the temperature is, the more intense the sub-cloud evaporation is, and the smaller the slope and intercept are (Craig, 1961). The LMWL of the summer half year (from March to September) was $\delta D=6.85\delta^{18}O-2.11$, and that of the winter half year (from October to February) was $\delta D=6.66\delta^{18}O-7.48$ (Fig. 2a). Some discrete points in Figure 2 were distributed on the right side of meteoric water line, indicating that there was a strong sub-cloud secondary evaporation in the study area. The slope of LMWL in summer was higher than that in winter, indicating more precipitation and higher relative humidity in summer than in winter in the study area. As shown in Figure 2b, the slope of LMWL in Kongtong District was 8.16, followed by Baiyin City (8.12), Wudu District (7.43), Yinchuan City (6.79), and Maqu County (4.68); and the intercept of LMWL in Kongtong District was 10.52, followed by Yinchuan City (0.75), Wudu District (–1.27), Baiyin City (–2.46), and Maqu County (–27.75). The equation of LMWL in the whole study area was $\delta D=7.34\delta^{18}O-1.16$ (Fig. 2c), which was lower than the global (Rozanski et al., 1993) and national (Wang et al., 2022) levels. This is mainly because of the low humidity and strong evaporation in arid area, which leads to the enrichment of stable δD and $\delta^{18}O$ isotopes in precipitation.

3.1.3 Environmental effect

Meteorological factors such as temperature, precipitation, and relative humidity are considered as the main environmental factors affecting the composition of precipitation isotope. Therefore, in this study, we discussed the relationship between $\delta^{18}O$ value in precipitation and meteorological factors at daily level. The results showed that there was a correlation between $\delta^{18}O$ value and temperature ($\delta^{18}O=0.24Tem-9.59$, $R^2=0.15$, $P<0.001$; Tem, temperature). The temperature effect for each sampling site was weaker than in the whole study area. There was a significant positive correlation between $\delta^{18}O$ value and temperature in Kongtong District ($R^2=0.13$, $P<0.050$). Maqu County is located in a continental alpine region with a low temperature throughout the year and a long cold season; in contrast, Wudu District has a high temperature throughout the year with sufficient precipitation and high relative humidity; we didn't find significant temperature effect at these two sampling sites. There was a significant negative correlation between $\delta^{18}O$ value and relative humidity in the margin area of East Asian monsoon ($\delta^{18}O=-0.16RH+5.09$, $R^2=0.18$, $P<0.001$; RH, relative humidity). A negative correlation was also found between $\delta^{18}O$ value and

precipitation ($\delta^{18}O$= –0.05Pre–5.82, R^2=0.01, P=0.104; Pre, precipitation), although the correlation between $\delta^{18}O$ value and precipitation at most sampling sites was not statistically significant at 0.05 level.

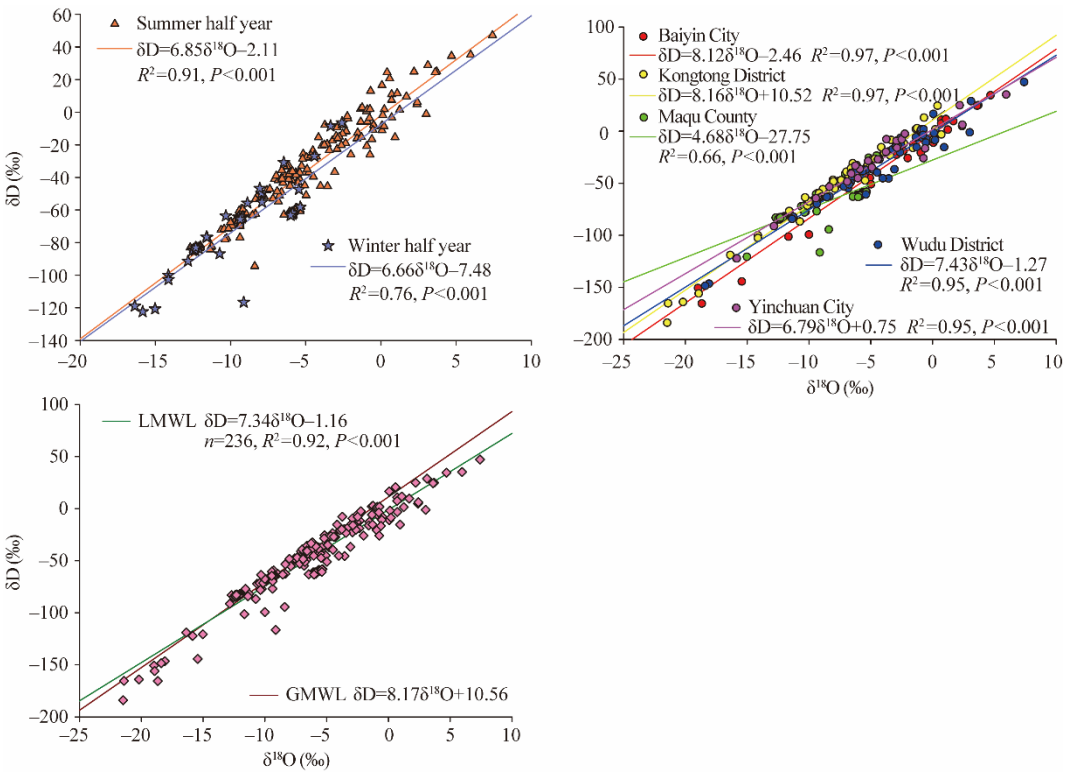

Fig. 2 Relationship between hydrogen (δD) value and oxygen ($\delta^{18}O$) value of precipitation in the study area in 2022. (a), relationship between δD value and $\delta^{18}O$ value of precipitation during summer half year and winter half year of 2022; (b), relationship between δD value and $\delta^{18}O$ value of precipitation at each sampling site in 2022; (c), relationship between δD value and $\delta^{18}O$ value of precipitation in the whole study area in 2022. LMWL, local meteoric water line; GMWL, global meteoric water line.

3.2 Backward trajectory analysis

The HYSPLIT-based backward trajectory model is considered as an effective method to simulate airflow movement. The backward duration for each trajectory was calculated as 10 d (240 h) before precipitation events, which is nearly the upper limit of the time that water vapor stays in air (Trenberth, 1998; Numaguti, 1999). The trajectory was calculated at 6-h intervals on the day of precipitation event occurred, that is, 00:00, 06:00, 12:00, and 18:00 (Beijing Time). We chose 1500 m above ground level as the start height for each sampling site. The Baiyin City and Wudu District were mainly affected by continental water vapor, and the northwest continental water vapor had the greatest influence for Baiyin City, accounting for 49.93% of the total water vapor (Fig. 3). The air mass in Kongtong District mainly came from the northwestern (37.36%), southeastern (23.70%), and western (23.28%) continent, and 15.66% of water vapor came from the Black Sea. The Maqu County was mainly affected by the westerlies, including 31.50% from the western continent, 28.68% from the Mediterranean Sea, and 13.82% from the Atlantic Ocean. In addition, Maqu County was also affected by water vapor from the southeast continent and the Indian Ocean. For Wudu District, the largest influence was from the western continent, accounting for 48.63% of the total water vapor. The Yinchuan City was mainly affected by water vapor from the northwest continent (78.70%), of which 24.32% of water vapor came from the direction of Russia. In addition, Yinchuan City was affected by a small part of local water vapor cycle (21.30%).

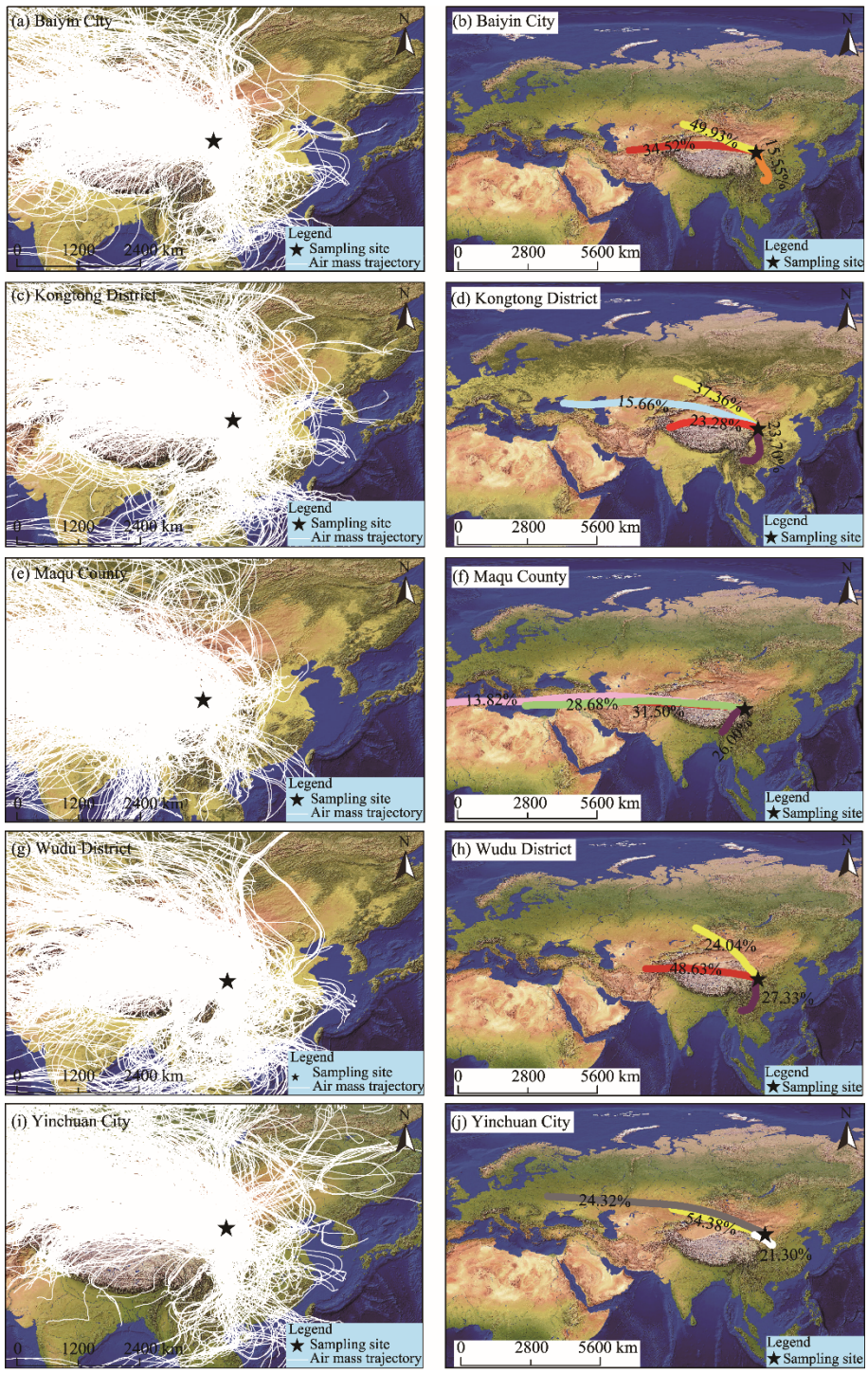

Fig. 3 Air mass trajectory (a, c, e, g, and i) and its clustering result (b, d, f, h, and j) at each sampling site in 2022. Different color lines in the right panel indicate that air mass comes from different directions; of which yellow line represents air mass comes from the northwest continent, grey line represents air mass comes from the northwest continent in the direction of Russia, red line represents air mass comes from the western continent, blue line represents air mass comes from the Black Sea, green line represents air mass comes from the Mediterranean, pink line represents air mass comes from the Atlantic Ocean, purple line represents air mass comes from the southwest continent, orange line represents air mass comes from the southeast continent, and white line represents air mass comes from the proximity continent. Note that the base map used for computerizing this map is from the Meteoinfo website (http://www.meteothink.org/index.html#).

3.3 Potential source area analysis

3.3.1 Identification of moisture sources

To further explore the sources of water vapor in the monsoon margin, we simulated the backward trajectories of 236 precipitation events from January to December 2022 in this study. Water samples were collected when every precipitation event occurred, and a precipitation event was defined as more than 1 mL of water was collected in this study. As the common operation in other studies, we took 10 d as the duration of trajectory before the occurrence of precipitation event. Based on the results of backward trajectory of HYSPLIT model, we divided the moisture sources of precipitation events into eight types (Table 3; Fig. 4): continental moisture from northwest (CNW), continental moisture from west (CW), continental moisture from proximity region (CP), continental moisture from southwest (CSW), continental moisture from southeast (CSE), moisture from the Indian Ocean to South China Sea (ITSC), moisture from the Atlantic Ocean (OA), and moisture from polar region (PR).

Table 3 Climatic, δD, and $\delta^{18}O$ characteristics of each kind of water vapor source for the monsoon margin in 2022

Water vapor source	*n*	Length (km)	v (m/s)	Tem (°C)	RH (%)	Pre (mm)	δD (‰)		$\delta^{18}O$ (‰)		*d*-excess (‰)	
							Mean	SD	Mean	SD	Mean	SD
CNW	33	7133	2.08	15.00	63.58	185.00	–23.24	31.65	–3.39	4.57	3.85	11.01
CW	76	6011	2.10	13.20	62.37	330.80	–39.83	37.70	–5.53	5.05	4.40	12.20
CP	13	3140	2.02	10.40	79.60	45.00	–46.30	28.14	–6.11	3.66	2.57	12.70
CSW	10	3152	2.19	9.70	76.50	31.80	–62.38	33.84	–8.22	5.62	3.38	13.86
CSE	9	3611	1.58	13.90	84.90	97.60	–36.88	22.38	–6.17	2.62	12.49	5.02
ITSC	79	5078	10.72	15.90	78.20	772.30	–58.28	24.81	–7.96	3.58	5.41	10.64
OA	10	16,815	2.30	8.60	70.79	37.90	–56.98	42.70	–7.54	5.62	3.32	12.14
PR	6	13,121	1.88	14.40	63.10	44.70	–9.55	23.41	–1.44	3.40	1.97	11.69

Note: *n* represents the number of precipitation events related to each kind of water vapor source in 2022. v, wind speed; Tem, temperature; RH; relative humidity; Pre, precipitation; SD, standard deviation; CNW, continental moisture from northwest; CW, continental moisture from west; CP, continental moisture from proximity; CSW, continental moisture from southwest; CSE, continental moisture from southeast; ITSC, moisture from the Indian Ocean to South China Sea; OA, moisture from Atlantic Ocean; PR, moisture from polar region.

For CNW, the average length of air mass trajectory was 7133 km. In 2022, 33 precipitation events related to CNW occurred, contributing 13.98% of the total 236 precipitation events in the monsoon margin, and such precipitation events were mainly concentrated in the summer half year (May–September). This part of air mass contributed about 12.00% of the total precipitation. This type of air mass originated from the northwest continent such as northern Siberia, Mongolia Plateau, and other regions, and extended to the study area; and it affected precipitation in the study area with partial local recycled water vapor. The air mass from this direction had low relative humidity, and high values of δD and $\delta^{18}O$, and brought little precipitation to the study area.

For CW, the average length of air mass trajectory was 6011 km. In 2022, there were 76 precipitation events related to CW, contributing 32.20% of the total number of precipitation events and 21.40% of the total precipitation in the monsoon margin. This type of air mass originated from Western Eurasia and extended to the study area by horizontal transport. It can be seen that the study area was mainly influenced by westerly air mass, from the results of backward trajectory clustering analysis done by this study. Especially in winter, CW contributed a high percentage of precipitation and a high relatively *d*-excess value.

For CP, the average length of air mass trajectory was 3140 km. In 2022, 13 precipitation events were related to CP, contributing 5.51% of the total number of precipitation events and 2.90% of the total precipitation in the monsoon margin. This kind of air mass was mainly from the continental area near the study area, and the precipitation events related to CP were mainly concentrated in the period around the monsoon (May–October). This part of the air mass had high relative humidity but produced little precipitation and the lowest *d*-excess value.

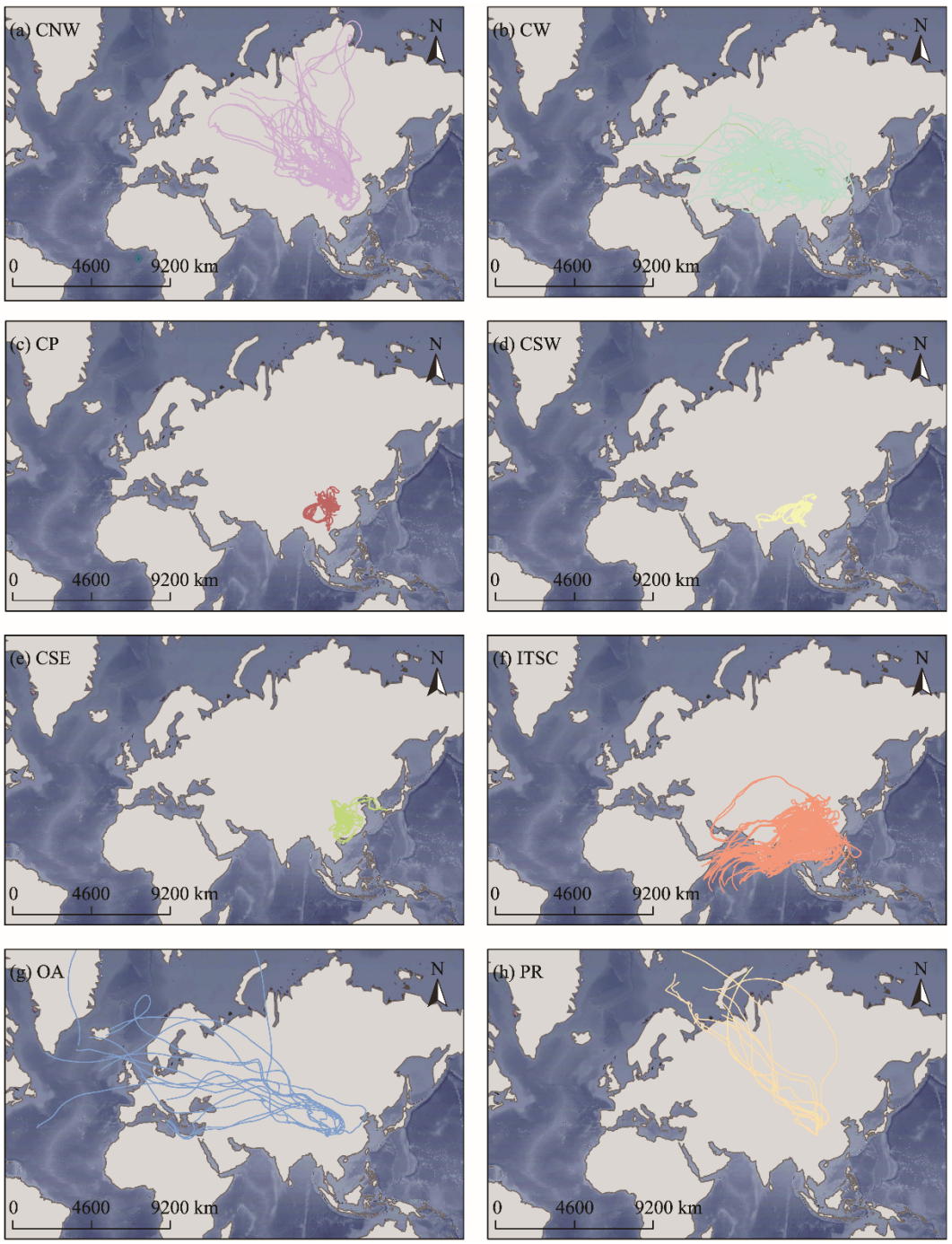

Fig. 4 Water vapor sources of precipitation in the monsoon margin in 2022. (a), continental moisture from northwest (CNW); (b), continental moisture from west (CW); (c), continental moisture from proximity region (CP); (d), continental moisture from southwest (CSW); (e), continental moisture from southeast (CSE); (f), moisture from the Indian Ocean to South China Sea (ITSC); (g), moisture from the Atlantic Ocean (OA); (h), moisture from polar region (PR). The denser the line, the more water vapor from this direction. Note that the base map used for computerizing this map is from the Meteoinfo website (http://www.meteothink.org/index.html#).

For CSW, the average length of air mass trajectory was 3152 km. In 2022, there were 10 precipitation events related to CSW, contributing 4.24% of the total 236 precipitation events and about 2.10% of the total precipitation in the monsoon margin. This kind of air mass was mainly

from the southwest continent near the study area like India and the Bay of Bengal. The precipitation was mainly concentrated in October after the summer monsoon. This part of air mass had high relative humidity and produced the lowest values of δD and $\delta^{18}O$.

For CSE, the average length of air mass trajectory was 3611 km. In 2022, 9 precipitation events related to CSE occurred, contributing 3.81% of the total number of precipitation events and about 6.30% of the total precipitation in the study area. This kind of air mass was mainly from the southeast continent of the study area and the Yellow Sea. Precipitation mainly came from the southeast monsoon, which happens in June–September each year. This part of air mass had high relative humidity, high temperature, and strong evaporation effect, and it produced the highest *d*-excess value.

For ITSC, the average length of air mass trajectory was 5078 km. In 2022, there were 79 precipitation events related to ITSC, contributing 33.47% of the total 236 precipitation events and about 50.00% of the total precipitation in the study area. This kind of air mass was mainly from the Indian Ocean, Arabian Sea, and South China Sea. Precipitation from this kind of air mass mainly dropped during June–September. At the beginning of monsoon period, carrying a lot of water vapor, air mass from ITSC passed through the southwest of China at a high speed and brought abundant precipitation to the study area. It usually had low values of δD and $\delta^{18}O$.

For OA, the average length of air mass trajectory was 16,815 km. In 2022, there were 10 precipitation events related to OA, contributing 4.24% of the total number of precipitation events and about 2.50% of the total precipitation in the study area. This type of air mass originated from the Atlantic Ocean and Mediterranean Sea and extended to the study area by zonal transport. Precipitation related with this kind of air mass mainly dropped during May–July. This kind of air mass had a relatively low humidity. However, the long-distance water vapor transportation caused the heavy isotopes in water vapor to be gradually consumed, resulting in a lower *d*-excess value.

For PR, the average length of air mass trajectory was 13,121 km. In 2022, 6 precipitation events related to PR occurred, contributing 2.54% of the total number of precipitation events and about 2.90% of the total precipitation in the study area. This type of air mass mainly originated from the Arctic Ocean and was transported to the study area through the northwest continent. Although it came from ocean, this type of air mass had low relative humidity, due to the long travel path. After passing over the Siberia and Mongolian Plateau, this kind of air mass had the lowest *d*-excess value.

3.3.2 Identification of water vapor source areas by PSCF and CWT

The PSCF analysis determined the magnitude of the impact of potential water vapor source areas, that is, the proportion of trajectories exceeding the threshold value of *d*-excess for each grid. Then CWT analysis was used to identify the magnitude of the weighted concentration values of potential evaporation source areas. The water vapor in Baiyin City mainly came from the west and southwest of the study area (Fig. 5). The water vapor in Kongtong District mainly came from the surrounding area and southwest direction. The precipitation sources in Maqu County were mainly distributed in the southwest of the study area. The water vapor in Wudu District mainly came from the south part. The water vapor sources of Yinchuan City were mainly distributed in the south and southeast. The results of CWT analysis showed that Baiyin City and Wudu District were mainly affected by CW and ITSC; while Kongtong District, Maqu County, and Yinchuan City were mainly affected by CP, ITSC, and CW.

3.3.3 Relationship between *d*-excess value and wind

The *d*-excess value responds to the climatic environment of water vapor source (Dansgaard, 1964). When the moisture source is relatively dry with low humidity and rapid evaporation, the *d*-excess value will be relatively high; conversely, the *d*-excess value will be relatively low (Malik et al., 2022). Figure 6 shows the relationship between *d*-excess value (interpolated using all precipitation events) and wind characteristics (wind speed and wind direction) for all precipitation events at the five sampling sites in 2022. High *d*-excess values in Baiyin City mainly appeared in

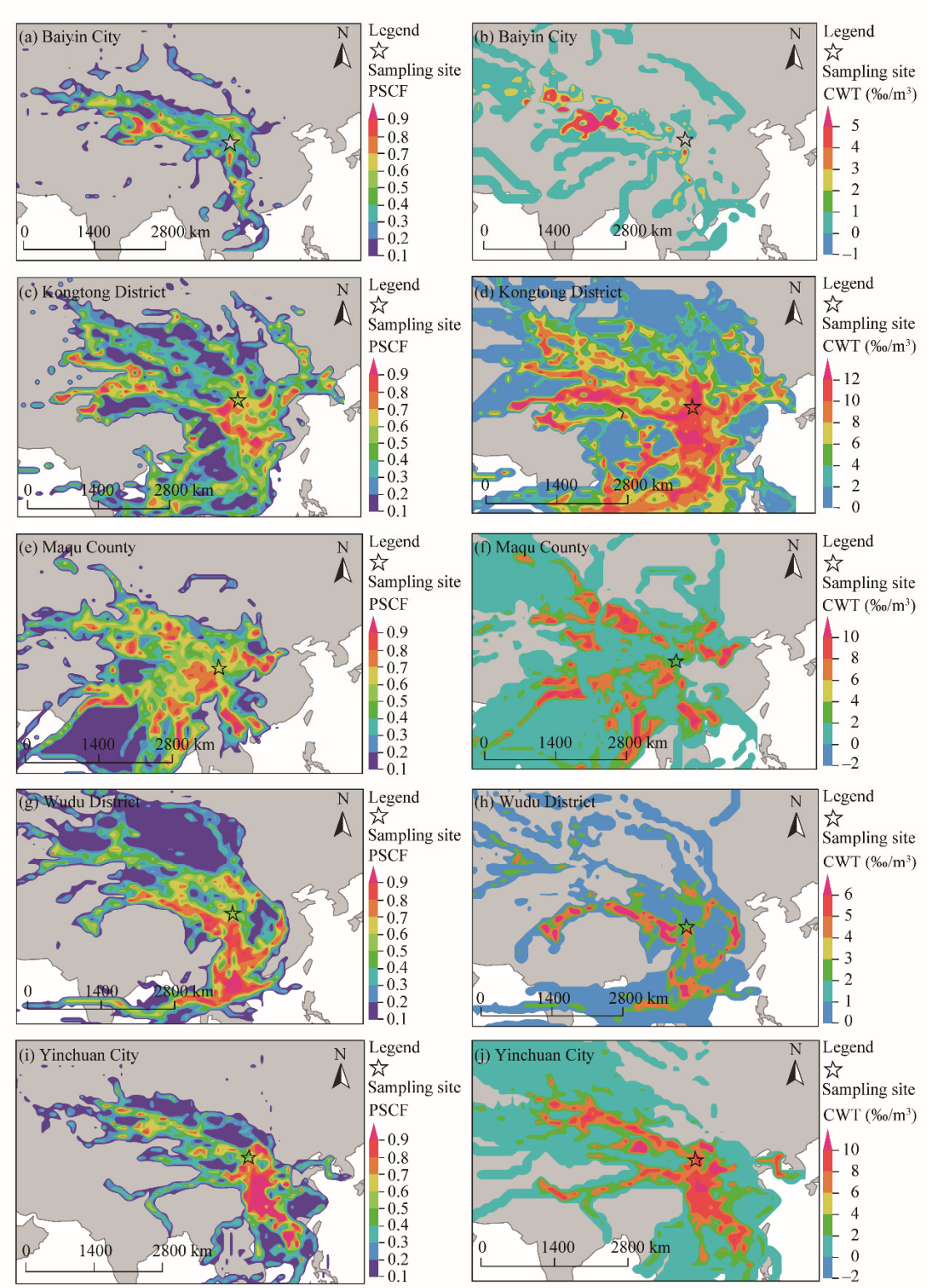

Fig. 5 Results of potential source contribution function (PSCF; a, c, e, g, and i) and concentration weighted trajectory (CWT; b, d, f, h, and j) for the potential water vapor source area analysis of the selected five sampling sites in the monsoon margin in 2022. Note that the base map used for computerizing this map is from the Meteoinfo website (http://www.meteothink.org/index.html#).

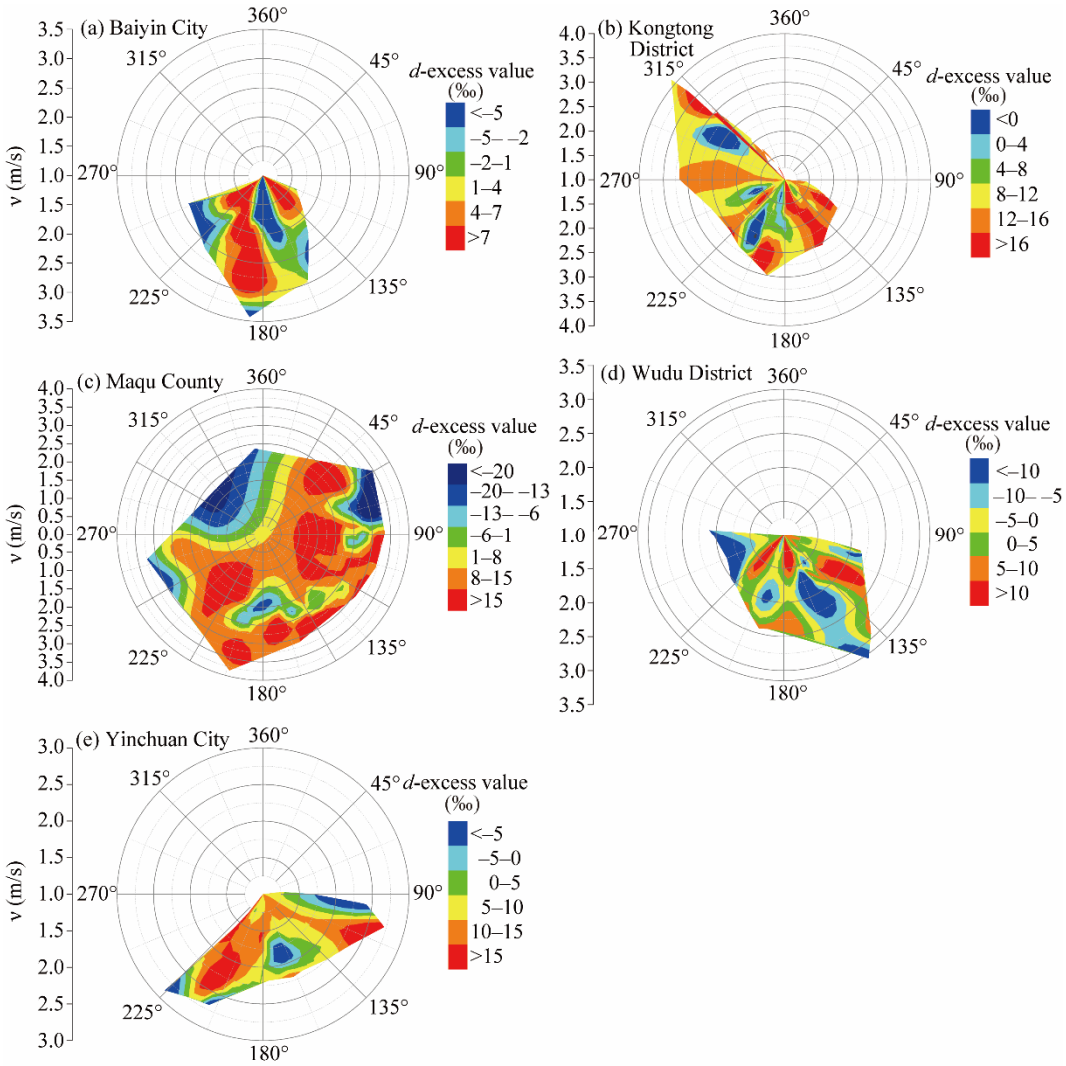

Fig. 6 Rose diagrams showing the relationship of deuterium excess (*d*-excess) value with wind speed (v) and direction at each sampling site. (a), Baiyin City; (b), Kongtong District; (c), Maqu County; (d), Wudu District; (e), Yinchuan City.

the precipitation of air mass blown from the south and southwest of China, and a small part of precipitation from the southeast of China when the wind speed is lower (<1.50 m/s). High *d*-excess values of Kongtong District mainly appeared in the precipitation of air mass blown from the southeast and southwest of China, with a small part from the northwest of China, when the wind speed is high (3.00–4.00 m/s). Precipitation was abundant in Maqu County, and high *d*-excess values mainly appeared in the precipitation of air mass originated from the southeast and southwest of China, and a small amount of precipitation from the northeast of China. High *d*-excess values of Wudu District mainly appeared in the precipitation of air mass originated from the southeast, south, and southwest of China with lower wind speed (<1.50 m/s). High *d*-excess values of Yinchuan City mainly appeared in the precipitation of air mass originated from the southeast and southwest of China.

4 Discussion

4.1 LWMN in the monsoon margin

The composition of δ^2H and $\delta^{18}O$ isotopes in precipitation air mass varies greatly, and the

difference of δ^2H and $\delta^{18}O$ isotopic composition can reflect the source of water vapor and the degree of water vapor evaporation (Claus et al., 2021; Bhat et al., 2022; Lekshmy et al., 2022). In this study, the equation of atmospheric water line in the western fringe of "monsoon triangle" was derived by the least square method. Compared with the GMWL, the slope of LMWL in the study area was relatively low. The results showed that the precipitation process was accompanied by secondary evaporation in the study area. In addition, the secondary evaporation was more intense in winter half year than in summer half year in the study area, according to the difference of *d*-excess value between these two periods, to be specific, the *d*-excess value of winter half year was lower than that of summer half year due to the lower relative humidity in winter.

4.2 Identification of water vapor sources

Precipitation in an area mainly consists of local evaporative water vapor and long-distance transported water vapor. Water vapor transported from outside the precipitation area is essential for the generation of intense precipitation (Zhao et al., 2023; Xie et al., 2023; Vishwakarma et al., 2024), especially for the northwest inland areas where air humidity is low, while evaporation is intense. Understanding the specific influence of different water vapor sources could better grasp the water cycle process in arid area. Zeng et al. (2020) found that westerly water vapor is the main water vapor in the northwest, which is consistent with the backward trajectory clustering results in this paper. According to the results of quantifying backward trajectory, the precipitation events related to CW and ITSC accounted for a large proportion. Due to low relative humidity, the precipitation events generated by CW in the study area were mostly drizzle or light rain. The water vapor carried by CW has evaporated almost completely in the long-distance transport process. The proportion of precipitation brought by ITSC was the highest, and the precipitation events were mainly concentrated in the monsoon period (from June to September). The air mass from ITSC, carrying a lot of water vapor, passed through the south and southwest of China at a high speed and brought a lot of precipitation to the northwest inland areas. Claus et al. (2021), Wu et al. (2021), and Wu and Bedaso (2022) deemed that the backward trajectory tracking method and second-order variable of isotopes (i.e., *d*-excess) could reflect the degree of imbalance in the evaporation-condensation process of water vapor source areas; and they also thought that *d*-excess could serve as an important indicator for tracing the source of water vapor. Based on the results of *d*-excess wind rose diagrams (Fig. 6), we found that precipitation in the monsoon margin was mainly influenced by monsoon moisture and westerly moisture. Although we set sampling sites in the monsoon margin, more sampling sites for a longer duration and larger spatial coverage are still needed in the future.

4.3 Influencing factors of precipitation isotopes

Dansgaard (1964) indicated the correlation between precipitation isotopes and environmental factors. The air humidity and temperature are important meteorological conditions for affecting precipitation isotopes (Wang et al., 2017; Li et al., 2022; Rhoujjati et al., 2023). We researched the correlation between precipitation isotopes and meteorological factors in this study and found that $\delta^{18}O$ value was positively correlated with temperature and negatively correlated with relative humidity in the study area. Compared with temperature and relative humidity, precipitation had a smaller correlation with the precipitation isotopes due to the low intensity of precipitation in the study area. The sources of water vapor are also considered to be important factors affecting the variation of precipitation isotope component (Tian et al., 2007; Crawford et al., 2013; Baker et al., 2015). We found that precipitation predominantly formed by dry continental water vapor tended to have higher *d*-excess value, while precipitation predominantly formed by moist marine water vapor tended to have lower *d*-excess value in the monsoon margin. In addition, the transport duration and distance of air mass are also vital to modify the isotopic component in precipitation. In this study, the relative humidity values of the air mass from CW, CNW, OA, and CP were 62.37%, 63.58%, 70.79%, and 79.60%, respectively (Table 3). The *d*-excess values of the four sources gradually decreased with the increase of air mass relative humidity. The *d*-excess value of

the precipitation from CSE was the highest (84.90%), which corresponds to its relatively high temperature and short transport path with less rainout. The air mass from ITSC had the highest temperature when compared with air mass from continental area, and the amount of precipitation from ITSC was relatively considerable. The heavy isotopes in water vapor are continuously eliminated throughout the transport path, as a result of air mass movement. Relative humidity was relatively low in the air mass from PR, CNW, and CW. With the extension of transport path, the *d*-excess value of the three areas steadily decreased.

5 Conclusions

In this study, we analyzed the precipitation isotope data gathered in the monsoon margin for the entire year 2022. Based on this, we used the HYSPLIT-based backward trajectory model, PSCF analysis, and CWT analysis to investigate the water vapor sources in the monsoon margin. The LMWL of the monsoon margin was $\delta D=7.34\delta^{18}O-1.16$, defined by regression analysis. The lower slope and intercept compared with the GMWL ($\delta D=8.17\delta^{18}O+10.56$) indicated the existence of strong regional evaporation in this area. Furthermore, the atmospheric water line slope of summer half year was higher than the slope of winter half year because of the high humidity in summer. We found that the effects of temperature (positive effect) and relative humidity (negative effect) to $\delta^{18}O$ value were significant through analyzing the relationship between the $\delta^{18}O$ value in precipitation and meteorological factors at daily level. The component of $\delta^{2}H$ and $\delta^{18}O$ isotopes was also greatly influenced by the air mass trajectory. Eight areas accounted for the majority of water vapor sources in the study area: CNW (13.98%), CW (32.20%), CP (5.51%), CSW (4.24%), CSE (3.81%), ITSC (33.47%), OA (4.24%), and PR (2.54%). The precipitation in the study area was mostly caused by the water vapor carried by ITSC because of the high moisture content of ITSC. Long water vapor transport distance increased the loss of precipitation isotopes. Understanding the atmospheric process of precipitation is important for managing water resource in arid and semi-arid areas. The research time of this study is relatively short (only one year), so the future study should take multi-year precipitation data to analyze the linkage between the composition of precipitation isotopes and water vapor sources in arid areas.

Competing interests

The authors declare that they have no known competing financial interests or personal relationships that could have appeared to influence the work reported in this paper.

Acknowledgements

This study was supported by the National Natural Science Foundation of China (42161007), the Scientific Research Program for Higher Education Institutions of Gansu Province (2021B-081), and the Natural Science Foundation of Gansu Province (22JR5RA074).

Author contributions

Conceptualization: CHEN Fenli, ZHANG Qiuyan; Data curation: ZHANG Qiuyan, GAO Minyan, CHEN Jufan; Methodology: CHEN Fenli, WANG Shengjie; Formal analysis: CHEN Fenli; Writing - original draft preparation: CHEN Fenli, ZHANG Qiuyan; Writing - review and editing: CHEN Fenli, ZHANG Qiuyan; Funding acquisition: CHEN Fenli, WANG Shengjie; Visualization: CHEN Fenli, WANG Shengjie, Mohd Aadil BHAT. All authors approved the manuscript.

References

Baker A J, Sodemann H, Baldini J U L, et al. 2015. Seasonality of westerly moisture transport in the East Asian summer monsoon and its implications for interpreting precipitation $\delta^{18}O$. Journal of Geophysical Research: Atmospheres, 120(12): 5850–5862.

Bian H, Ying Z, Li T, et al. 2017. Interannual variability in the onset of the South China Sea summer monsoon from 1997 to

2014. Atmospheric and Oceanic Science Letters, 10(1): 73–81.

Bhat M A, Zhong J, Dar T, et al. 2022. Spatial distribution of stable isotopes in surface water on the upper Indus River basin (UIRB): Implications for moisture source and paleoelevation reconstruction. Applied Geochemistry, 136: 105137, doi: 10.1016/j.apgeochem.2021.105137.

Breitenbach S F M, Adkins J F, Meyer H, et al. 2010. Strong influence of water vapor source dynamics on stable isotopes in precipitation observed in Southern Meghalaya, NE India. Earth and Planetary Science Letters, 292(1–2): 212–220.

Cai Z Y, Tian L D, Bowen G J. 2018. Spatial-seasonal patterns reveal large-scale atmospheric controls on Asian Monsoon precipitation water isotope ratios. Earth and Planetary Science Letters, 503: 158–169.

Chen F L, Zhang M J, Argiriou A A, et al. 2020. Deuterium excess in precipitation reveals water vapor source in the monsoon margin sites in Northwest China. Water, 12(12): 3315, doi: 10.3390/w12123315.

Chen J H, Li Y, Xiong B, et al. 2023. Comparison of moisture sources of summer precipitation in 1998 and 2020 in the middle and lower reaches of Yangtze River basin. International Journal of Climatology, 43(8): 3493–3505.

Claus K, Rolf F R, Fernando R B, et al. 2021. Vapour source and spatiotemporal variation of precipitation isotopes in Southwest Spain. Hydrological Processes, 35(12): e14445, doi: 10.1002/hyp.14445.

Cloux S, Garaboa-Paz D, Insua-Costa D, et al. 2021. Extreme precipitation events in the Mediterranean area: contrasting two different models for moisture source identification. Hydrology and Earth System Sciences, 25(12): 6465–6477.

Craig H. 1961. Isotopic variations in meteoric waters. Science, 133: 1702–1703.

Crawford J, Hughes C E, Parkes S D. 2013. Is the isotopic composition of event based precipitation driven by moisture source or synoptic scale weather in the Sydney Basin, Australia? Journal of Hydrology, 507: 213–226.

Dansgaard W. 1964. Stable isotopes in precipitation. Tellus, 16(4): 436–468.

Espinoza J C, Arias P A, Moron V, et al. 2021. Recent changes in the atmospheric circulation patterns during the dry-to-wet transition season in south tropical South America (1979–2020): impacts on precipitation and fire season. Journal of Climate, 34(22): 9025–9042.

Fang L J, Gao R Z, Wang X X, et al. 2022. Isotopes-based characterization of precipitation compositions and atmospheric water vapor sources over typical Eurasian steppes in south Mongolian Plateau. Journal of Hydrology, 615: 128724, doi: 10.1016/j.jhydrol.2022.128724.

Geppert M, Hartmann K, Kirchner I, et al. 2022. Precipitation over Southern Africa: moisture sources and isotopic composition. Journal of Geophysical Research: Atmospheres, 127(21): e2022JD037005, doi: 10.1029/2022JD037005.

Gimeno L, Stohl A, Trigo R M, et al. 2012. Oceanic and terrestrial sources of continental precipitation. Reviews of Geophysics, 50: RG4003, doi: 10.1029/2012RG000389.

Gou J F, Qu S M, Guan H D, et al. 2022. Relationship between precipitation isotopic compositions and synoptic atmospheric circulation patterns in the lower reach of the Yangtze River. Journal of Hydrology, 605: 127289, doi: 10.1016/j.jhydrol.2021.127289.

Hsu Y K, Holsen M T, Hopke P K. 2003. Comparison of hybrid receptor models to locate PCB sources in Chicago. Atmospheric Environment, 37(4): 545–562.

Jiao Y M, Liu C J, Gao X, et al. 2019. Impacts of moisture sources on the isotopic inverse altitude effect and amount of precipitation in the Hani Rice Terraces region of the Ailao Mountains. Science of the Total Environment, 687: 470–478.

Kong Y L, Wang K, Pan S, et al. 2023. Effect of moisture sources on the isotopic composition of precipitation in Northwest China. Water, 15(8): 1584, doi: 10.3390/w15081584.

Kurita N. 2013. Water isotopic variability in response to mesoscale convective system over the tropical ocean. Journal of Geophysical Research: Atmospheres, 118(18): 10376–10390.

Lee J E, Fung I, DePaolo D J, et al. 2007. Analysis of the global distribution of water isotopes using the NCAR atmospheric general circulation model. Journal of Geophysical Research: Atmospheres, 112(D16): 306, doi: 10.1029/2006JD007657.

Lekshmy P R, Midhun M, Ramesh R. 2022. Role of moisture transport from Western Pacific region on water vapor isotopes over the Bay of Bengal. Atmospheric Research, 265: 105895, doi: 10.1016/j.atmosres.2021.105895.

Li J J, Feng Z D, Tang L Y. 1988. Late quaternary monsoon patterns on the Loess Plateau of China. Earth Surface Processes and Landforms, 13(2): 125–135.

Li X Y, Kawamura R, Sugimoto A, et al. 2022. Isotopic composition and moisture sources of precipitation in midlatitude regions characterized by extratropical cyclones' route. Journal of Hydrology, 612: 128047, doi: 10.1016/j.jhydrol.2022.128047.

Lone A M, Achyuthan H, Chakraborty S, et al. 2020. Controls on the isotopic composition of daily precipitation characterized by dual moisture transport pathways at the monsoonal margin region of North-Western India. Journal of Hydrology, 588: 125106, doi: 10.1016/j.jhydrol.2020.125106.

Ma L, Sun Y B, Jin Z D, et al. 2022. Magnesium isotopic evidence for staged enhancement of the East Asian Summer Monsoon precipitation since the Miocene. Geochimica et Cosmochimica Acta, 324: 140–155.

Malik F, Butt S, Mujahid N. 2022. Variation in isotopic composition of precipitation with identification of vapor source using deuterium excess as tool. Journal of Radioanalytical and Nuclear Chemistry, 331: 683–690.

Moore M, Kuang Z, Blossey P N. 2014. A moisture budget perspective of the amount effect. Geophysical Research Letters, 41(4): 1329–1335.

Natali S, Doveri M, Giannecchini R, et al. 2022. Is the deuterium excess in precipitation a reliable tracer of moisture sources and water resources fate in the western Mediterranean? New insights from Apuan Alps (Italy). Journal of Hydrology, 614: 128497, doi: 10.1016/j.jhydrol.2022.128497.

Numaguti A. 1999. Origin and recycling processes of precipitating water over the Eurasian continent: Experiments using an atmospheric general circulation model. Journal of Geophysical Research: Atmospheres, 104(D2): 1957–1972.

Pant N, Semwal P, Khobragade S D, et al. 2021. Tracing the isotopic signatures of cryospheric water and establishing the altitude effect in Central Himalayas: A tool for cryospheric water partitioning. Journal of Hydrology, 595: 125983, doi: 10.1016/j.jhydrol.2021.125983.

Pérez-Alarcón A, Sorí R, Fernández-Alvarez J C, et al. 2023. Moisture source for the precipitation of tropical cyclones over the Pacific Ocean through a Lagrangian Approach. Journal of Climate, 36(4): 1059–1083.

Rhoujjati N, Ait Brahim Y, Hanich L, et al. 2023. Precipitation isotopes to elucidate moisture sources in the Western Mediterranean: case of the Middle Atlas Mountains, Morocco. Environmental Earth Sciences, 82: 250, doi: 10.1007/S12665-023-10930-2.

Risi C, Bony S, Vimeux F. 2008. Influence of convective processes on the isotopic composition ($\delta^{18}O$ and δD) of precipitation and water vapor in the tropics: 2. Physical interpretation of the amount effect. Journal of Geophysical Research: Atmospheres, 113(D19): 306, doi: 10.1029/2008JD009943.

Rozanski K, Araguás-Araguás L, Gonfiantini R. 1993. Isotopic patterns in modern global precipitation. In: Swart P K, Lohmann K C, Mckenzie J, et al. Climate Change in Continental Isotopic Records, Volume 78. Geophysical Monograph Series. Hoboken: AGU (American Geophysical Union) Publications, 1–36.

Salamalikis V, Argiriou A A, Dotsika E. 2016. Periodicity analysis of $\delta^{18}O$ in precipitation over Central Europe: Time–frequency considerations of the isotopic 'temperature' effect. Journal of Hydrology, 534: 150–163.

Shi Y D, Wang S J, Wang L W, et al. 2010. Isotopic evidence in modern precipitation for the westerly meridional movement in Central Asia. Atmospheric Research, 259: 105698, doi: 10.1016/j.atmosres.2021.105698.

Steen-Larsen H C, Sveinbjörnsdottir A E, Jonsson T, et al. 2015. Moisture sources and synoptic to seasonal variability of North Atlantic water vapor isotopic composition. Journal of Geophysical Research: Atmospheres, 120(12): 5757–5774.

Stohl A, Forster C, Frank A, et al. 2005. Technical note: The Lagrangian particle dispersion model FLEXPART version 6.2. Atmospheric Chemistry and Physics, 5(9): 2461–2474.

Sun C J, Zhou S J, Jing Z W. 2023. Variability of precipitation-stable isotopes and moisture sources of two typical landforms in the eastern Loess Plateau, China. Journal of Hydrology: Regional Studies, 46: 101349, doi: 10.1016/j.ejrh.2023.101349.

Tan M. 2014. Circulation effect: response of precipitation $\delta^{18}O$ to the ENSO cycle in monsoon regions of China. Climate Dynamics, 42: 1067–1077.

Tang Y, Song X F, Zhang Y H, et al. 2017. Using stable isotopes to understand seasonal and interannual dynamics in moisture sources and atmospheric circulation in precipitation. Hydrological Processes, 31(26): 4682–4692.

Tao X, Pang H X, Zhan Z J, et al. 2023. Characteristics of water vapor isotopes and moisture sources for short-duration heavy rainfall events in Nanjing, eastern China. Journal of Hydrology, 622: 129731, doi: 10.1016/j.jhydrol.2023.129731.

Tharammal T, Bala G, Nusbaumer J M. 2023. Sources of water vapor and their effects on water isotopes in precipitation in the Indian monsoon region: a model-based assessment. Scientific Reports, 13: 708, doi: 10.1038/s41598-023-27905-9.

Tian L, Yao T, MacClune K, et al. 2007. Stable isotopic variations in west China: A consideration of moisture sources. Journal of Geophysical Research: Atmospheres, 112(D10): 12, doi: 10.1029/2006JD007718.

Trenberth K E. 1998. Atmospheric moisture residence times and cycling: Implications for rainfall rates and climate change. Climatic Change, 39: 667–694.

Vishwakarma V, Pattnaik S, Baisya H. 2024. Decadal variability of precipitation and moisture source attribution over India. International Journal of Climatology, 4(2): 703–719.

Wang Q Y. 2014. MeteoInfo: GIS software for meteorological data visualization and analysis. Meteorological Applications, 21(2): 360–368.

Wang S J, Zhang M J, Crawford J, et al. 2017. The effect of moisture source and synoptic conditions on precipitation isotopes in arid central Asia. Journal of Geophysical Research: Atmospheres, 122(5): 2667–2682.

Wang S J, Lei S J, Zhang M J, et al. 2022. Spatial and seasonal isotope variability in precipitation across China: Monthly isoscapes based on regionalized fuzzy clustering. Journal of Climate, 35(11): 3411–3425.

Worden J, Noone D, Bowman K. 2007. Importance of rain evaporation and continental convection in the tropical water cycle. Nature, 445: 528–532.

Wu S Y, Bedaso Z. 2022. Quantifying the effect of moisture source and transport on the precipitation isotopic variations in northwest Ethiopian Highland. Journal of Hydrology, 605: 127322, doi: 10.1016/j.jhydrol.2021.127322.

Wu X X, Chen F L, Liu X Y, et al. 2021. The significance of hydrogen and oxygen stable isotopes in the water vapor source in Dingxi Area. Water, 13(17): 2374, doi: 10.3390/w13172374.

Xie C, Zhao L J, Eastoe C J, et al. 2022. Precipitation stable isotope composition, moisture sources, and controlling factors in Xi'an, Northwest China. Atmospheric Research, 280: 106428, doi: 10.1016/j.atmosres.2022.106428.

Xie X X, Liu X D. 2023. Contributions of terrestrial and oceanic moisture sources to orbital-scale precipitation variations over the northern East Asian monsoon region. Global and Planetary Change, 229: 104244, doi: 10.1016/j.gloplacha.2023.104244.

Yang Q C, Mu H K, Guo J C, et al. 2019. Temperature and rainfall amount effects on hydrogen and oxygen stable isotope in precipitation. Quaternary International, 519: 25–31.

Yao T D, Masson-Delmotte V, Gao J, et al. 2013. A review of climatic controls on $\delta^{18}O$ in precipitation over the Tibetan Plateau: Observations and simulations. Reviews of Geophysics, 51(4): 525–548.

Zannoni D, Steen-Larsen H C, Rampazzo G, et al. 2019. The atmospheric water cycle of a coastal lagoon: An isotope study of the interactions between water vapor, precipitation and surface waters. Journal of Hydrology, 572: 630–644.

Zeng D, Wu J K, Li H Y, et al. 2020. Progress of hydrogen and oxygen isotope studies in precipitation in the Northwest Arid Zone. Arid Zone Research, 37(4): 857–869. (in Chinese)

Zeng Y, Hopke P K. 1989. A study of the sources of acid precipitation in Ontario, Canada. Atmospheric Environment, 23(7): 1499–1509.

Zhang M M, Jia W X, Zhu G F, et al. 2023. The effect of the seasonality of moisture sources on moisture flux and precipitation stable isotopes in the Shiyang River Basin. Theoretical and Applied Climatology, 151: 767–783.

Zhao N, Wu P, Manda A, et al. 2023. Moisture sources of the Tohoku heavy rainfalls in August 2022 and the influences of tropical storms. Geophysical Research Letters, 50(17): e2023GL104166, doi: 10.1029/2023GL104166.

Zhou H, Zhang X P, Yao T C, et al. 2019. Variation of $\delta^{18}O$ in precipitation and its response to upstream atmospheric convection and rainout: A case study of Changsha station, south-central China. Science of the Total Environment, 659: 1199–1208.